Improving Lubrication Efficiency at High Sliding Speeds by Plasma Surface Texturing

Wei Zha, Jingzeng Zhang, Chen Zhao, Ran Cai, Xueyuan Nie

Abstract—Cathodic plasma electrolysis (CPE) is used to create surface textures on cast iron samples for improving the tribological properties. Micro craters with confined size distribution were successfully formed by CPE process. These craters can generate extra hydrodynamic pressure that separates two sliding surfaces, increase the oil film thickness and accelerate the transition from boundary to mixed lubrication. It was found that the optimal crater size was 1.7 μm, at which the maximum lubrication efficiency was achieved. The Taguchi method was used to optimize the process parameters (voltage and roughness) for CPE surface texturing. The orthogonal array and the signal-to-noise ratio were employed to study the effect of each process parameter on the coefficient of friction. The results showed that with higher voltage and lower roughness, the lower friction coefficient can be obtained, and thus the lubrication can be more efficiently used for friction reduction.

Keywords—Cathodic plasma electrolysis, friction, lubrication, plasma surface texturing.

I. INTRODUCTION

FRICTION and wear are the severe problems which significantly influence the energy consumption [1] and lifetime [2] of the mechanical components. Hard coating is conventionally applied to reduce the friction and wear by thermal spray [3]-[5], electroplating [6] and hot dipping [7]. But some limitations are related with these techniques such as high cost, complicated process, inability to treat workpieces with irregular shapes and the environmentally unfriendly electrolytes [8]. The use of lubricant is an effective method to control wear and friction. Lubrication could be divided into three regimes: boundary, mixed and hydrodynamic (elastohydrodynamic) lubrication [9]. In boundary lubrication, the two sliding surfaces fully contact with each other and the friction is completely determined by the properties of the surfaces, such as roughness, skewness and kurtosis [10]. In mixed lubrication, the oil film thickness boosts to a value that is high enough to partially support the applied load and the friction is determined by the properties of lubricant and asperities together [11]. In hydrodynamic lubrication, the two sliding surfaces are completely separated by the lubricant. Since no asperities contact occur, the friction is only related to the viscosity of lubricant and the wear can be almost avoided [12]. Similar to hydrodynamic lubrication, in elastohydrodynamic lubrication the lubricant fully supports the applied load. However, since the extremely high pressure is applied, the significant elastic deformation of the surfaces occurs and influences the thickness of the lubricant film [13].

For last decades, surface texturing was developed to improve the efficiency of lubrication and thus more effectively reduce the wear and friction [14]. The effects of surface texturing vary when the sliding system is in different lubrication regimes. The craters act as micro reservoirs for lubricant so that when two surfaces slide in boundary lubrication, the lubricant can be supplied from the craters to the sliding interface, although the lubricant is squeezed out from the contact region due to the high pressure [11]. Besides that, the craters can trap the wear debris to prevent the severe abrasive wear until they are filled [15]. In hydrodynamic lubrication, the negative pressure in the diverging region of a dimple is limited by the cavitation, while the positive pressure in the converging region is not limited, leading to the positive net pressure that support the applied load [16], [17]. Above effects work together in mixed lubrication to reduce the friction and wear [18].

So far, surface texturing has been applied in many fields to control the friction, such as cutting tools [19]-[21], mechanical seals [22]-[24], journal bearings [25]-[27], cylinder liners [28]-[30] and piston rings [31]-[33]. The textured surface exhibits low friction coefficient and high wear resistance. Laser surface texturing [34], [35] is one of the most popular techniques that are being used. It can produce accurate textures with the help of computer software. However, the expensive high-energy-laser sources, complicated control software, and masks used to create the certain patterned textures limit the application of Laser surface texturing in massive industrial production. Micro-electric discharging machining [20] and chemical etching [36] could produce surface textures without changing the mechanical properties of the workpieces or causing no harm to the target surface, but the material removal rate is low.

This paper aims to apply CPE on cast iron samples to improve their tribological behavior. During CPE surface texturing process, the surfaces of cast iron samples (cathode) are covered by the gas bubbles, resulting in the accumulation of the electrons. The applied voltage across the electrodes mainly drops in the gaseous envelope, generating high electric field. As the electric field strength reaches to a critical value (106 ~ 108 V/m), the gas starts to ionize, forming uniformly distributed plasma discharges on the whole sample surface [37]. Heated by the extremely high temperature plasma core (6000-8000 K) [38], the gas bubbles explode melting the metal surface and forming the craters. The effects of applied voltages and surface roughness on the friction coefficient are studied by the Taguchi method. The relationship between the crater size and the

Wei Zha, Jingzeng Zhang, Chen Zhao, Ran Cai, Xueyuan Nie are with Department of Mechanical, Automotive & Materials Engineering, University of Windsor, Windsor, ON, N9B 3P4, Canada

Xueyuan Nie is with Department of Mechanical, Automotive & Materials Engineering, University of Windsor, Windsor, ON, N9B 3P4, Canada (corresponding author, phone: 519-253-3000; e-mail: xnie@uwindsor.ca).

lubrication efficiency is also investigated.

II. EXPERIMENTAL DETAILS

A. Sample Preparation

Cast iron (Fe: 93%, C: 3%, Mg: 0.8%, P: 0.1%, Si: 2%, S: 0.05%) rings (outer diameter: 100 mm and inner diameter: 70 mm) were polished with grit 1200 sand papers and ultra-sonic cleaned with acetone. As shown in Fig. 1, during CPE process the sample and the nozzle acted as cathode and anode, respectively. The electrolyte (25-30 g/L Na_2CO_3 dissolved in deionized water) was pumped (1.5 L/min) to the nozzle and uniformly sprayed to the sample surface. The cathodic plasma discharging process was conducted for 60 s under DC mode at 180 V (at which the plasma discharges initiated), 200 V and 220 V (above which abnormal arcing occurred), respectively. The gap between the nozzle and sample surface was set to be about 6 mm. When uniform plasma envelope was built, the current density was 1.5 A/cm^2. During the whole process, the temperature of the electrolyte was kept at 35-40 ℃ with the chiller. A blank sample with no treatment was also prepared as a reference. The roughness of samples prepared at 180, 200 and 220 V were 0.80, 1.01 and 1.25 μm, respectively.
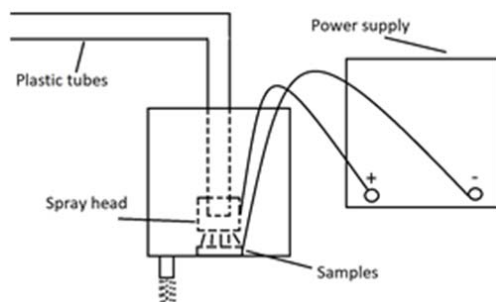

Fig. 1 Experimental setup of CPE

B. Tribotests

For the tribotests, all samples were polished to three levels of surface roughness: 0.7, 0.6 and 0.5 μm. The surface morphologies were observed with the optical microscope. The crater size was obtained from the microscopic images with a photo analysis software. The tribological behavior of the CPE surface textured samples were studied by the Pin-on-disk sliding tester. The rotational speed of the tester could reach 960 rpm corresponding to sliding velocity of about 4.5 m/s. All the tests were conducted at room temperature with SAE 5W20 as the lubricant. AISI 52100 steel balls (62 HRC, 6 mm in diameter) were used as pins with a normal load of 5 N. During the tribotests, the sliding velocity increased from 0 to 4.5 m/s, and the coefficient of friction (COF) vs. sliding velocity curves were recorded.

III. RESULTS

A. Surface Morphology

The surface morphologies of CPE surface textured samples after polishing are shown in Fig. 2. As demonstrated in Fig. 2 (a), the crater size was very small at 180 V, which was the critical voltage for initiation of the plasma. Thus, the energy of the gas bubble explosion was not high enough to generate large craters. As the voltage increased by 20 V, the crater size increased to about 1.8 μm, as illustrated in Fig. 2 (b). However, occasionally large crater with diameter of 4 μm could be found in Fig. 2 (c) when the voltage increased to 220 V. Under such high voltage, more electrons accumulated on the gas bubbles, leading to the high energy explosion. It has been verified that the crater size of the sample treated by higher voltage was larger than the one treated by lower voltage after they are polished to the same roughness. Similar results can be observed in Figs. 2 (d)-(f) and (g)-(i).
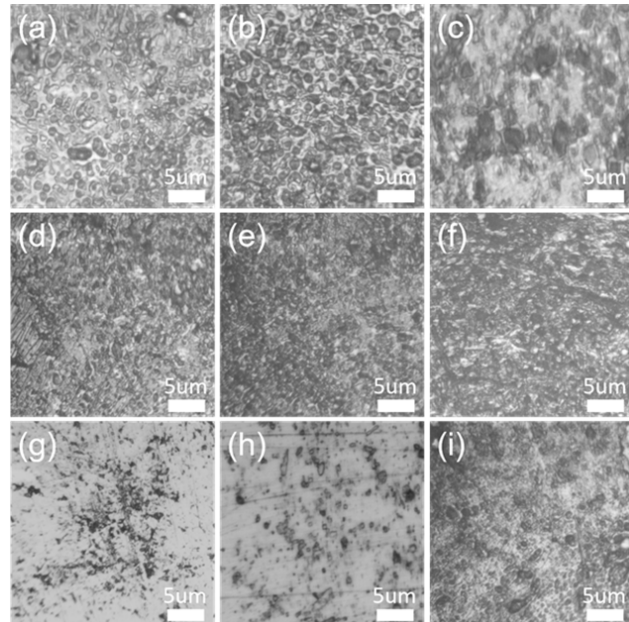

Fig. 2 The surface morphologies of CPE treated samples polished to obtain the roughness of 0.7 μm at (a) 180 V, (b) 200 V and (c) 220 V; the surface morphologies of CPE treated samples polished to obtain the roughness of 0.6 μm at (d) 180 V, (e) 200 V and (f) 220 V; the surface morphologies of CPE treated samples polished to obtain the roughness of 0.5 μm at (g) 180 V, (h) 200 V and (i) 220 V

B. Frictional Behaviour

The COF vs. sliding velocity curve of the reference sample is shown in Fig. 3 (a). It can be found that although the velocity increased from 0 to 4.5 m/s, the COF barely decreased, which means the tribosystem was working in boundary lubrication. Figs. 3 (b)-(d) show the COF vs. velocity curves of CPE surface textured samples. When the velocity was very low, the COF stayed at a relatively high value indicating that the lubricating system was in the boundary regime. As the velocity increased, the COF dropped steeply, and the lubrication was transitioned into mixed regime. At maximum sliding velocity, the COF still decreased but with a much lower rate, which means the tribosystem was still in mixed lubrication but going to enter elastohydrodynamic lubrication (EHL) if the velocity kept increasing. It was noticed that at certain velocity, the COF of each sample was different. The lowest value of COF of each

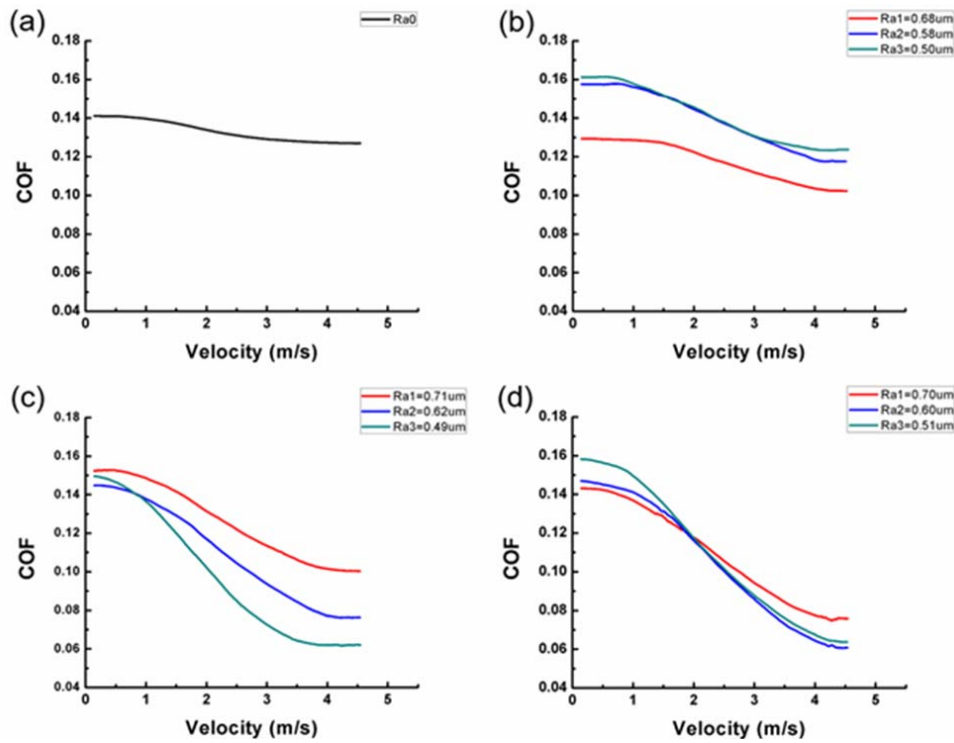sample was collected and used as the responses for Taguchi design.

Fig. 3 The COF vs. Sliding velocity curves of (a) reference, (b)-(d) CPE treated samples at 180 V, 200 V and 220 V

C. Taguchi Design

Run	Voltage (V)	Roughness (μm)	Lowest COF	S/N ratio
1	180	0.68	0.108	19.33
2	180	0.58	0.125	18.06
3	180	0.50	0.130	17.72
4	200	0.71	0.090	20.91
5	200	0.62	0.075	22.49
6	200	0.49	0.060	24.43
7	220	0.70	0.075	22.49
8	220	0.60	0.058	24.73
9	220	0.51	0.060	24.43

Fig. 4 The results for COFs and S/N ratios

To select an appropriate orthogonal array, the total degrees of freedom of process parameter s (applied voltage and surface roughness) need to be calculated first. In this work, each process parameter had three levels. So the degree of freedom of each parameter was 2. Since the interaction between the process parameters was neglected, the total degrees of freedom were 4. Basically, the degrees of freedom for the orthogonal array should be larger than that of the process parameters. So a L9 orthogonal array was chosen. Only nine experiments needed to be conducted to study the entire combination of the process parameters.
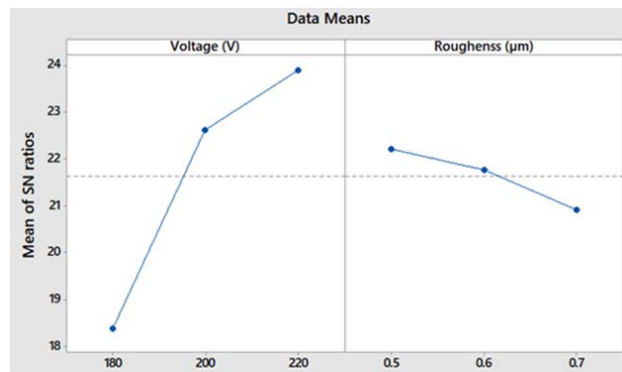

Fig. 5 Plots of effects of main S/N ratios

To obtain optimal friction performance, the lower-the-better formula: $S/N = -10\log(y^2)$ for COF was used [39]. The experimental results for COF and corresponding S/N ratio are shown in Fig. 4. The effect of each process parameter at different levels can be separated out by taking the mean value of S/N ratio for the certain level. The mean S/N ratio for 180 V, 200 V and 220 V can be calculated by taking the average of the S/N ratio for the experiments 1-3, 4-6 and 7-9, respectively. The mean S/N ratio for each level of roughness can be

computed in the same way. Fig. 5 shows the mean S/N ratio graph for COF. It can be found that the mean S/N ratio increases non-linearly with the increase of voltage and the decrease of roughness. When the voltage increased from 180 V to 200 V, the mean S/N ratio dramatically increased. But when the voltage increased to 220 V, the mean S/N ratio increased slowly. It indicates that there might be an optimal value of crater size that results in the lowest COF.

IV. DISCUSSION

Hamrock and Dowson [40] proposed to calculate the film thickness between two smooth sliding surfaces with an empirical equation:

$$h_c = 2.69 U^{0.67} G^{0.53} W^{-0.067} \left[1 - 0.61 \exp\left(-0.73 D^{-2/\pi} \right) \right]$$

where the dimensionless speed parameter $U = \frac{u\eta_0}{E'R_x}$, the dimensionless load parameter $W = \frac{\omega}{E'R_x^k}$ and the dimensionless load parameter $G = \alpha E'$. In the current work, dynamic viscosity of lubricant η_0 is 0.1, the effective elastic modulus of the surfaces $E^{\wedge\prime}$ is 68.3 GPa, reduced radius of curvature R_x is $5.35 \times 10\text{-}5$ m, The external load ω is 5 N, k is 2 for elliptical contact, lubricant pressure-viscosity coefficient α is 1.3×108.

The film thickness ratio $\lambda = h_c/R_a$ was developed to determine in which lubrication regimes the sliding system is [41] where hc is film thickness and Ra is surface roughness. If $\lambda < 1$, it is in boundary lubrication; if $1 < \lambda < 3$, it is in mixed lubrication; and if $\lambda > 3$, it is in hydrodynamic lubrication. For the reference sample (Ra = 0.16), the film thickness ratio was calculated as $\lambda = 0.85$ even the sliding speed goes up to 4.5 m/s, which verifies that the reference sample stayed in boundary lubrication during the whole tribotest.

The λ of those CPE surface textured samples were also less than 1 for the whole velocity range, but the drastic decrease of COF along with increasing sliding velocity indicated that those tribosystems had already entered mixed lubrication. This phenomenon could be explained by the extra hydrodynamic pressure generated by the craters, which were not considered in Hamrock and Dowson's theory. This extra hydrodynamic pressure could lift the counterpart, so that the film thickness would increase even the speed was not very high. Therefore, the divergence between the experimental results and Hamrock and Dowson's theory represented the strength of extra hydrodynamic pressure and could be used to scale the effectiveness of the surface texturing that can improve the lubrication efficiency. To evaluate the divergence, the critical film thickness ratio λc, at which the transition between boundary and mixed lubrication occurred, was calculated based on the COF vs. sliding velocity curves. The lower λc, the higher divergence and thus the higher lubrication efficiency. The curve of λc vs. crater size is shown in Fig. 6. It can be found that the λc value of all samples was much less than 1, which means that surface texturing can significantly improve the lubrication efficiency. Moreover, as the crater size increased, the λc decreased to about 0.1 and then increases to about 0.16. Thus,

the optimal crater size was about 1.7 µm. If the crater size is less than this value, the hydrodynamic pressure is weaker and can only support the two sliding surfaces at higher speed. N If the crater size is larger than that, the film becomes unstable since the deep craters might destroy the film.
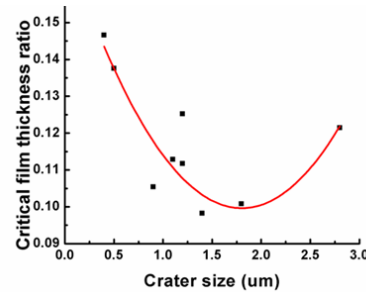

Fig. 6 Mapping nonlinear data to a higher dimensional feature space

V. CONCLUSION

CPE was used to produce surface textures on cast iron samples. The Taguchi experimental design was used to investigate the optimal process parameters (applied voltage and roughness) that resulted in the lowest COF at high sliding speed. It was concluded that the lower COF could be obtained at higher voltage and lower roughness. Since a larger crater size produced by a higher voltage could generate a larger hydrodynamic pressure, the result of the enlarged crater could lead to occurrence of separation of the sliding contact surfaces shifting to a lower sliding velocity. In contrast to a rougher cratered surface, a smooth surface would benefit the formation and stability of lubricant film. The optimal voltage and roughness were 220 V and 0.5 µm analyzed by the S/N ratio diagram where a minimum COF of about 0.06 could be obtained at velocity of 4.5 m/s. The critical film thickness ratio λc at which the tribosystem was transitioned from boundary to mixed lubrication was used to determine the lubrication efficiency. Better lubrication efficiency could be obtained if lower critical film thickness ratio was calculated, since the tribosystem was transitioned into mixed lubrication at lower velocity. It was concluded that the lubrication efficiency was improved for all CPE surface textured samples compared with the untextured one. Increasing the crater size could improve the lubrication efficiency before the highest value was obtained at optimal crater size of about 1.7 µm. After that, the further increase in the crater size would lead to the decrease of lubrication efficiency.

REFERENCES

[1] K. Holmberg, P. Andersson, and A. Erdemir, "Global energy consumption due to friction in passenger cars." Tribology International 47 (2012): 221-234.
[2] M. Dubar, M., A. Dubois, and L. Dubar, "Wear analysis of tools in cold forging: PVD versus CVD TiN coatings." Wear 259.7-12 (2005):

1109-1116.

[3] N. Espallargas, J. Berget, J. M. Guilemany, A.V. Benedetti, and P. H. Suegama, "Cr3C2–NiCr and WC–Ni thermal spray coatings as alternatives to hard chromium for erosion–corrosion resistance." Surface and Coatings Technology 202, no. 8 (2008): 1405-1417.

[4] M. P. Nascimento, R. C. Souza, I. M. Miguel, W. L. Pigatin, and H. Voorwald, "Effects of tungsten carbide thermal spray coating by HP/HVOF and hard chromium electroplating on AISI 4340 high strength steel." Surface and coatings technology 138, no. 2-3 (2001): 113-124.

[5] D. Toma, W. Brandl, and G. Marginean, "Wear and corrosion behaviour of thermally sprayed cermet coatings." Surface and coatings technology 138, no. 2-3 (2001): 149-158.

[6] J. R.Tuck, A. M. Korsunsky, R. I. Davidson, S. Bull, and D. M. Elliott, "Modelling of the hardness of electroplated nickel coatings on copper substrates." Surface and Coatings Technology 127, no. 1 (2000): 1-8.

[7] E. Frutos, J. L. González–Carrasco, C. Capdevila, J. A. Jiménez, and Y. Houbaert, "Development of hard intermetallic coatings on austenitic stainless steel by hot dipping in an Al–Si alloy." Surface and Coatings Technology203, no. 19 (2009): 2916-2920.

[8] V. S. Protsenko, and F. I. Danilov, "Chromium electroplating from trivalent chromium baths as an environmentally friendly alternative to hazardous hexavalent chromium baths: comparative study on advantages and disadvantages." Clean Technologies and Environmental Policy 16, no. 6 (2014): 1201-1206.

[9] Y. Yan, "Tribology and tribo-corrosion testing and analysis of metallic biomaterials." In Metals for Biomedical Devices, pp. 178-201. Woodhead Publishing, 2010.

[10] S. H. Loring, R. E. Brown, A. Gouldstone, and J. P. Butler, "Lubrication regimes in mesothelial sliding." Journal of Biomechanics 38, no. 12 (2005): 2390-2396.

[11] X.B. Lu, and M. M. Khonsari, "An experimental investigation of dimple effect on the stribeck curve of journal bearings." Tribology letters 27, no. 2 (2007): 169.

[12] L. Galda, P. Pawlus, and J. Sep, "Dimples shape and distribution effect on characteristics of Stribeck curve." Tribology International 42, no. 10 (2009): 1505-1512.

[13] K. L. Johnson, "Regimes of elastohydrodynamic lubrication." Journal of Mechanical Engineering Science 12, no. 1 (1970): 9-16.

[14] I. Etsion, "State of the art in laser surface texturing." In ASME 7th Biennial Conference on Engineering Systems Design and Analysis, pp. 585-593. American Society of Mechanical Engineers, 2004.

[15] M. Varenberg, G. Halperin, and I. Etsion, "Different aspects of the role of wear debris in fretting wear." Wear 252, no. 11-12 (2002): 902-910.

[16] M. Fowell, A. V. Olver, A. D. Gosman, H. A. Spikes, and I. Pegg, "Entrainment and inlet suction: two mechanisms of hydrodynamic lubrication in textured bearings." Journal of Tribology 129, no. 2 (2007): 336-347.

[17] M. Scaraggi, "Textured surface hydrodynamic lubrication: Discussion." Tribology Letters 48, no. 3 (2012): 375-391.

[18] D. Braun, C. Greiner, J. Schneider, and P. Gumbsch, "Efficiency of laser surface texturing in the reduction of friction under mixed lubrication." Tribology international 77 (2014): 142-147.

[19] N. Kawasegi, H. Sugimori, H. Morimoto, N. Morita, and I. Hori, "Development of cutting tools with microscale and nanoscale textures to improve frictional behavior." Precision Engineering 33, no. 3 (2009): 248-254.

[20] P. Koshy, P., and J. Tovey, "Performance of electrical discharge textured cutting tools." CIRP annals 60, no. 1 (2011): 153-156.

[21] T. Sugihara, and T. Enomoto, "Crater and flank wear resistance of cutting tools having micro textured surfaces." Precision Engineering 37, no. 4 (2013): 888-896.

[22] X. Su, L. Shi, W. Huang, and X. L. Wang, "A multi-phase micro-abrasive jet machining technique for the surface texturing of mechanical seals." The International Journal of Advanced Manufacturing Technology 86, no. 5-8 (2016): 2047-2054.

[23] D. Gropper, L. Wang, and T. J. Harvey, "Hydrodynamic lubrication of textured surfaces: A review of modeling techniques and key findings." Tribology International94 (2016): 509-529.

[24] M. Adjemout, A. Andrieux, J. Bouyer, N. Brunetière, G. Marcos, and T. Czerwiec, "Influence of the real dimple shape on the performance of a textured mechanical seal." Tribology International 115 (2017): 409-416.

[25] N. Tala-Ighil, and M. Fillon, "A numerical investigation of both thermal and texturing surface effects on the journal bearings static characteristics." Tribology International 90 (2015): 228-239.

[26] T. Ibatan, M. S. Uddin, and M. A. K. Chowdhury, "Recent development on surface texturing in enhancing tribological performance of bearing sliders." Surface and Coatings Technology 272 (2015): 102-120.

[27] Y. Henry, J. Bouyer, and M. Fillon, "An experimental analysis of the hydrodynamic contribution of textured thrust bearings during steady-state operation: a comparison with the untextured parallel surface configuration." Proceedings of the Institution of Mechanical Engineers, Part J: Journal of Engineering Tribology 229, no. 4 (2015): 362-375.

[28] W. Grabon, P. Pawlus, S. Wos, W. Koszela, and M. Wieczorowski, "Effects of honed cylinder liner surface texture on tribological properties of piston ring-liner assembly in short time tests." Tribology International 113 (2017): 137-148.

[29] X. J. Hua, J. G. Sun, P. Zhang, H. Ge, Y. Fu, J. Ji, and B. Yin, "Research on discriminating partition laser surface micro-texturing technology of engine cylinder." Tribology International 98 (2016): 190-196.

[30] N. Morris, R. Rahmani, H. Rahnejat, P. D. King, and S. Howell-Smith, "A numerical model to study the role of surface textures at top dead center reversal in the piston ring to cylinder liner contact." Journal of Tribology 138, no. 2 (2016): 021703.

[31] A. B. Zavos, and P. G. Nikolakopoulos, "Simulation of piston ring tribology with surface texturing for internal combustion engines." Lubrication Science 27, no. 3 (2015): 151-176.

[32] A. Akbarzadeh, and M. Khonsari, "Effect of untampered plasma coating and surface texturing on friction and running-in behavior of piston rings." Coatings 8, no. 3 (2018): 110.

[33] C. X. Gu, X. Meng, Y. Xie, and Y. Yang, "Effects of surface texturing on ring/liner friction under starved lubrication." Tribology international 94 (2016): 591-605.

[34] D. Q. He, S. Zheng, J. Pu, G. Zhang, and L. Hu, "Improving tribological properties of titanium alloys by combining laser surface texturing and diamond-like carbon film." Tribology international 82 (2015): 20-27.

[35] A. A. Voevodin, and J. S. Zabinski, "Laser surface texturing for adaptive solid lubrication." Wear 261, no. 11-12 (2006): 1285-1292.

[36] P. O. Papet, A. Nichiporuk, Y. R. Kaminski, J. Kraiem, J-F. Lelievre, A. Chaumartin, A. Fave, and M. Lemiti, "Pyramidal texturing of silicon solar cell with TMAH chemical anisotropic etching." Solar Energy Materials and Solar Cells 90, no. 15 (2006): 2319-2328.

[37] A. L. Yerokhin, X. Nie, A. Leyland, A. Matthews, and S. J. Dowey, "Plasma electrolysis for surface engineering." Surface and coatings technology 122, no. 2-3 (1999): 73-93.

[38] R. O. Hussein, X. Nie, D. O. Northwood, A. Yerokhin, and A. Matthews, "Spectroscopic study of electrolytic plasma and discharging behaviour during the plasma electrolytic oxidation (PEO) process." Journal of Physics D: Applied Physics 43, no. 10 (2010): 105203.

[39] H. Atil, and Y. Unver, "A different approach of experimental design: Taguchi method." Pakistan Journal of Biological Sciences 3, no. 9 (2000): 1538-1540.

[40] B. J. Hamrock, and D. Dowson, "Isothermal elastohydrodynamic lubrication of point contacts: part III—fully flooded results." Journal of Lubrication Technology 99, no. 2 (1977): 264-275.

[41] B. J. Hamrock, S. R. Schmid, and B. O. Jacobson, Fundamentals of fluid film lubrication. CRC press, 2004. "Synthetic structure of industrial plastics (Book style with paper title and editor)," in Plastics, 2nd ed. vol. 3, J. Peters, Ed. New York: McGraw-Hill, 1964, pp. 15–64.